

The proton radius puzzle

This article has been downloaded from IOPscience. Please scroll down to see the full text article.

2011 J. Phys.: Conf. Ser. 312 032002

(<http://iopscience.iop.org/1742-6596/312/3/032002>)

View [the table of contents for this issue](#), or go to the [journal homepage](#) for more

Download details:

IP Address: 129.187.254.47

The article was downloaded on 23/02/2012 at 06:29

Please note that [terms and conditions apply](#).

The proton radius puzzle

A Antognini^{1,2}, F D Amaro³, F Biraben⁴, J M R Cardoso³,
D S Covita⁵, A Dax⁶, S Dhawan⁶, L M P Fernandes³, A Giesen⁷,
T Graf⁸, T W Hänsch^{1,9}, P Indelicato⁴, L Julien⁴, C-Y Kao¹⁰,
P Knowles¹¹, F Kottmann², E-O Le Bigot⁴, Y-W Liu¹⁰,
J A M Lopes³, L Ludhova¹¹, C M B Monteiro³, F Mulhauser¹¹,
T Nebel¹, F Nez⁴, P Rabinowitz¹², J M F dos Santos³,
L A Schaller¹¹, K Schuhmann⁷, C Schwob⁴, D Taqqu¹³,
J F C A Veloso⁵ and R Pohl¹

¹ Max-Planck-Institut für Quantenoptik, 85748 Garching, Germany.

² Institut für Particle Physics, ETH, 8093 Zurich Switzerland.

³ Departamento de Física, Universidade de Coimbra, 3004-516 Coimbra, Portugal.

⁴ LKB, École Normale Supérieure, CNRS and Université P. et M. Curie, 75252 Paris, France.

⁵ I3N, Departamento de Física, Universidade de Aveiro, 3810-193 Aveiro, Portugal.

⁶ Physics Department, Yale University, New Haven, CT 06520-8121, USA.

⁷ Dausinger & Giesen GmbH, 70178 Stuttgart, Germany.

⁸ Institut für Strahlwerkzeuge, Universität Stuttgart, 70569 Stuttgart, Germany.

⁹ Ludwig-Maximilians-Universität, Munich, Germany.

¹⁰ Physics Department, National Tsing Hua University, Hsinchu 300, Taiwan.

¹¹ Département de Physique, Université de Fribourg, 1700 Fribourg, Switzerland.

¹² Department of Chemistry, Princeton University, Princeton, NJ 08544-1009, USA.

¹³ Paul Scherrer Institut, 5232 Villigen-PSI, Switzerland.

E-mail: aldo.antognini@psi.ch

Abstract. By means of pulsed laser spectroscopy applied to muonic hydrogen (μ^-p) we have measured the $2S_{1/2}^{F=1} - 2P_{3/2}^{F=2}$ transition frequency to be 49881.88(76) GHz [1]. By comparing this measurement with its theoretical prediction [2, 3, 4, 5, 6, 7] based on bound-state QED we have determined a proton radius value of $r_p = 0.84184(67)$ fm. This new value differs by 5.0 standard deviations from the CODATA value of 0.8768(69) fm [8], and 3 standard deviation from the e-p scattering results of 0.897(18) fm [9]. The observed discrepancy may arise from a computational mistake of the energy levels in μp or H, or a fundamental problem in bound-state QED, an unknown effect related to the proton or the muon, or an experimental error.

1. Introduction

The hydrogen atom (H) is unique as physical theories can be applied to it “without” approximations. Any discrepancy between theoretical prediction and experimental measurement which may be unveiled at any increase of theoretical and experimental accuracy thus holds the potential for new fundamental insights.

Nothing can hide in H, not even the proton at its center. In fact, measurements with hydrogen beams by Stern in 1933 revealed that the magnetic moment of the proton deviated from the prediction of the Dirac relativistic theory. This was the first indication that the proton - contrary to the electron - has a structure. In 1947 measurements of the 2S-2P splitting (Lamb shift) and

1S-hyperfine splitting in H deviated from those predicted by the Dirac equation. This was the initiation for the development of quantum electrodynamics (QED). In the last four decades, the goal to measure H energy levels with greater accuracy has led to advances in high resolution spectroscopy and metrology. This peaked with the invention of the frequency comb laser. The high accuracy obtained with such techniques provided cornerstones to test bound-state QED, to determine the Rydberg constant R_∞ and the proton radius (assuming the correctness of the theory), and to search for slow time variations of fundamental constants.

Hydrogen energy levels are slightly modified by the fact that in contrast to the electron the proton has a finite size. Hence, to precisely predict these energy levels an accurate knowledge of the root-mean-square charge radius of the proton (r_p) is necessary. The historical method of determining r_p was based upon scattering electrons on protons, in effect by scattering an electron beam on a liquid hydrogen target. The uncertainty related to the knowledge of r_p extracted from electron-proton scattering limited the prediction accuracy of the H energy levels, and consequently it was limiting the comparison between theory and measurements. Therefore to advance the check (comparison between prediction and measurement) of bound-state QED describing the H energy levels it was necessary to have a more precise determination of r_p . This was one of the main motivations for our experiment: to measure the 2S-2P splitting (Lamb shift) in muonic hydrogen (μp) with 30 ppm accuracy in order to determine r_p with a precision better than 0.1%. This is a factor of 20 improvement compared with the value from scattering experiments and thus paves the way to check H theory, more precisely the 1S Lamb shift, a factor of 20 better as previously achievable.

The muon is about 200 times heavier than the electron. As a consequence the μp atomic Bohr radius is correspondingly smaller than in H. Effects of the finite size of the proton on the μp energy levels are thus enhanced. For hydrogen-like atoms the finite size effect *i.e.* the energy shift caused by the fact that the proton has a finite size is given in leading order by [4]

$$\Delta E^{FS} = \frac{2(Z\alpha)^4}{3n^3} m_r^3 r_p^2 \delta_{l0} \quad (1)$$

where Z is the nuclear charge number, α the fine-structure constant, n the principal quantum number, m_r the reduced mass of the system and δ_{l0} the Kronecker symbol. Only S-states ($l = 0$) are thus shifted in leading order. ΔE^{FS} in μp is 10^7 larger than in H because of the m_r^3 dependence. Therefore by measuring the $\mu p(2S - 2P)$ transition frequency even with moderate accuracy it is possible to extract r_p with great accuracy.

2. Experimental principle

Our experiment is based upon laser spectroscopy of μp and therefore two main components are necessary: a low energy muon beam and a laser system.

Muonic hydrogen is produced by stopping negative muons (μ^-) in H_2 gas. The μp atoms are produced at highly excited states (around $n \sim 14$). Most of these de-excite quickly to the 1S-ground state, but $\sim 1\%$ populate the long-lived 2S-state (Fig. 1 (a)) whose lifetime is 1 μs at 1 hPa gas pressure [10, 11]. A short laser pulse tunable to a wavelength around $\lambda \approx 6 \mu m$ (corresponding to $\mu p(2S - 2P)$ splitting) illuminates the muonic atom. $2S \rightarrow 2P$ transitions are induced by the laser light (Fig. 1 (b)), immediately (lifetime of the 2P state is $\tau_{2P} = 8.5$ ps) followed by $2P \rightarrow 1S$ de-excitation via emission of a Lyman K_α X-ray of 1.9 keV energy. Obviously, the transition from the 2S to the 2P state and the subsequent emission of X-ray only occurs if the laser frequency is resonant with the 2S-2P transition. A resonance curve is obtained by measuring the number of 1.9 keV X-rays at different laser wavelengths that occur in time-coincidence with the laser pulse.

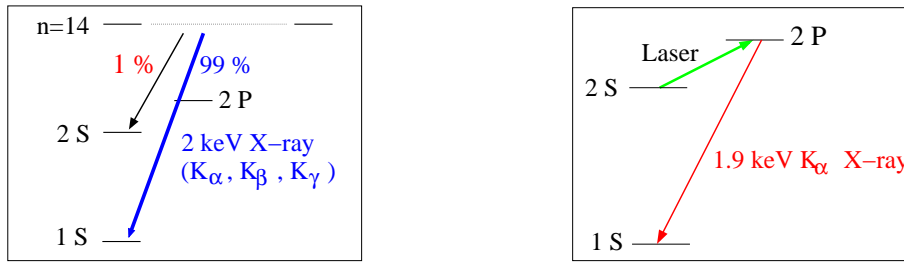


Figure 1. (a) μp atom formation. About 99% of the μ^- stopped in H_2 cascade directly (within 100 ns at 1 hPa gas pressure) emitting X-rays of the Lyman series at around 2 keV. 1% of the μ^- populate the long-lived metastable 2S state whose lifetime is $\tau_{2S} = 1 \mu s$ at 1 hPa H_2 gas. (b) The μp atoms are illuminated by a laser pulse 1 μs after formation. If the laser is on resonance, K_α X-rays in time coincidence with the laser pulse are observed.

3. Low energy muon beam

The μp Lamb shift experiment requires to stop μ^- in a H_2 target at 1 hPa pressure and in a reasonably small volume (pencil-like) which can be efficiently illuminated by the laser light. Thus μ^- with kinetic energies of ~ 5 keV are needed. Low H_2 gas pressure is required to have a long-lived $\mu p(2S)$ population, *i.e.* to reduce collisional quenching of the 2S-state.

Our muon beam shown in Fig. 2 consists of the Cyclotron Trap (CT) [12] for the production of low energy μ^- , the muon extraction channel (MEC) which is a curved solenoid for the transport and the selection of μ^- with 2 MeV/c momentum, and a 1 m long solenoid (PSC) containing two non-destructive μ^- transmission detectors and the H_2 gas target.

10^8 sec^{-1} negative pions (π^-) with a momentum of 102 MeV/c enter the CT tangentially, where they are moderated by passing a degrader. The position (radial: $r \sim 10$ cm) and thickness (5.4 g/cm^2) of the moderator are chosen such that the π^- have a precession trajectory when they exit the moderator which minimizes the chance of a second hit on the moderator. After moderation the π^- have a momentum of 40 – 60 MeV/c, *i.e.* near the “magic momentum” of 40 MeV/c. About 30% of the moderated π^- decay in flight into μ^- before returning back to the moderator or hitting the wall of the target vessel. Only a few percent of these μ^- have suitable momenta and angles accepted by the magnetic quasi-potential-well (radial and axial) formed by the CT field. Muons confined radially and axially are moderated when crossing a thin Formvar foil of $20 \mu\text{g/cm}^2$ (160 nm) thickness and 17 cm diameter placed in the median plane of the CT (see Fig. 2 (b)). Muons produced at kinetic energies of a few MeV are thus decelerated within their lifetime to 10 – 50 keV and then extracted from the CT.

The axial magnetic confinement can be understood by considering the magnetic flux invariance $p_\perp^2/B = \text{const}$ (adiabatic approximation) where p_\perp is the transverse muon momentum. The “magnetic bottle” has a field minimum $B_0 \simeq 2$ T in the center of the trap at $z = 0$. Therefore when the muon moves away from the magnetic field minimum, its axial momentum is transferred into radial momentum till the axial momentum reaches zero and the muon is back reflected towards the center of the trap. Thus the CT is a magnetic trap for particles which satisfy the condition

$$\left| \frac{p_\parallel(0)}{p_\perp(0)} \right| < \left(\frac{B_{\text{max}}}{B_0} - 1 \right)^{1/2} \quad (2)$$

where $p_\parallel(0)$ is the axial momentum in the trap center and $B_{\text{max}} \simeq 4$ T the maximal magnetic field at the coil centers. The foil in the CT center is metalized with 3 nm of Ni and put at high negative voltage ($V = -19$ kV). The additional electric potential modifies the trapping

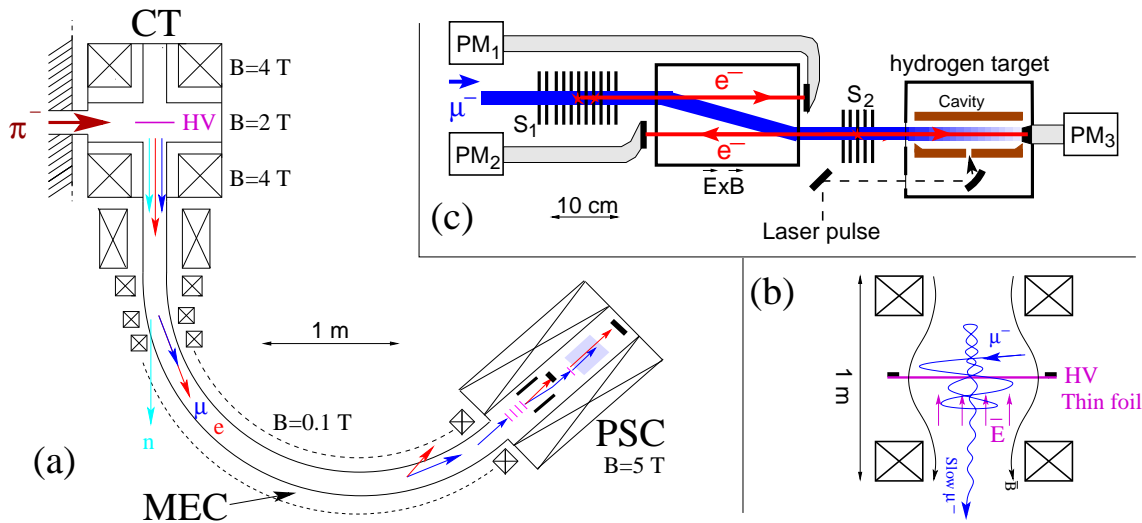


Figure 2. (a) Layout of the $\pi E5$ area at PSI with Cyclotron Trap (CT), muon extraction channel (MEC), and PSC solenoid. (b): Schematic view of a μ^- trajectory in the CT. A metalized thin foil in the trap center moderates the μ^- during their lifetime. The foil being at high voltage defines also the axial electric field for μ^- extraction. (c) Schematic view of the apparatus mounted inside the 5 T PSC solenoid. The μ^- enters two stacks of ultra-thin carbon foils, S_1 and S_2 , which act together with PM_1 , PM_2 and PM_3 as muon detector. The $\vec{E} \times \vec{B}$ filter (shown in side view) separates μ^- from e^- . The H_2 gas target of 1 hPa pressure is separated by the vacuum of the muon beam line by a 30 nm thick Formvar foil. The laser cavity mirrors (shown in top view) are placed sideways of the muon stop volume. The laser light enters the multi-pass mirror cavity through a hole in one of the cavity mirrors. Two LAAPD arrays are mounted above and below the muon stop volume (not shown in the picture).

condition as

$$\frac{T_{\parallel}(0)}{T_{\perp}(0)} < \left(\frac{B_{\max}}{B_0} - 1 \right) - \frac{qV}{T_{\perp}(0)} \quad (3)$$

where $T_{\parallel}(0)$ and $T_{\perp}(0)$ are respectively the axial and radial kinetic energies at the trap center, and q the muon charge ($qV > 0$). On average a μ^- crosses the foil several hundred times and at every crossing it loses energy. When the transverse component $T_{\perp}(0)$ is sufficiently small (see Eq. (3)) the μ^- escapes from the CT trap.

The escaping μ^- enter the MEC, a toroidal momentum filter assembled from normal conducting magnetic coils (magnetic field $B = 0.15\text{ T}$). Since the MEC magnetic field has a “small” horizontal gradient (toroidal shape), the charged particles undergo a small vertical drift (out of the plane in Fig. 2) relative to the magnetic field lines. Particles with different momenta undergo different vertical drifts and thus momentum selection can be achieved by placing collimators at the correct vertical positions. Monte Carlo simulations showed that 2 MeV/c particles undergo a maximal vertical drift relative to the magnetic field lines of about $\sim 4.5\text{ cm}$, whereas the high flux of keV energy electrons (low momentum $p_e \sim 0.14\text{ MeV}/c$ for 20 keV energy) have an almost negligible vertical drift. This vertical drift caused by the gradient of the magnetic field in horizontal direction can be understood qualitatively as being the consequence of different gyration radii ($= -p_{\perp}/qB$) as the particle moves in and out of regions of larger than average and smaller than average magnetic field strengths.

From the MEC, the μ^- are guided into the bore hole of a 5 Tesla superconducting PSC

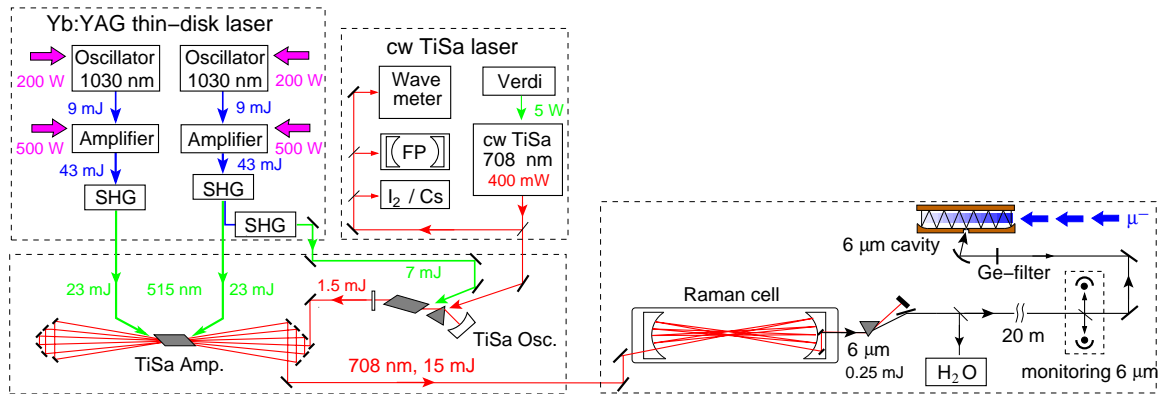


Figure 3. A frequency doubled Yb:YAG thin-disk laser pumps an oscillator-amplifier TiSa laser. The oscillator is frequency controlled by an injection seeding from a frequency stabilized cw TiSa laser. The pulses from the TiSa laser are shifted to $6 \mu\text{m}$ with a Raman process and then transported from the laser hut to the multi-pass cavity surrounding the μ^- stop volume.

magnet whose strong field ensures minimal radial size of the muon beam. The setup inside the PSC solenoid is shown in Fig. 2 (c). Before entering the H_2 target, the μ^- pass two stacks (S_1 and S_2) of ultra-thin carbon foils ($d = 4 \mu\text{g}/\text{cm}^2$ for each foil) kept at high electric potential which both serve as muon detectors and decelerate the μ^- to 5 keV. Each μ^- releases a few e^- in the stack-foils which are separated from the much slower μ^- in an $\vec{E} \times \vec{B}$ separator field. The e^- are detected by plastic scintillators read out by PMT and their coincidence provide the trigger signal for the laser systems. The number of detected μ^- is 330 s^{-1} at a proton beam current of $1900 \mu\text{A}$. The S_1 and S_2 detector efficiencies are 80% and 70% respectively. The trigger quality, *i.e.* the fraction of stopped to detected μ^- , is $Q \approx 40\%$ at 1 hPa.

Finally, the μ^- enters the H_2 target. The μ^- stopping volume has a length of 20 cm and $5 \times 12 \text{ mm}^2$ transverse dimension. Above and below, two arrays (2×10) of Large Area Avalanche Photo-Diodes record the 1.9 keV K_α X-rays. They have an active area of $14 \times 14 \text{ mm}^2$ with energy resolution of 25% (FWHM), time resolutions of 40 ns (FWHM), and detection efficiency of $\sim 80\%$ for 1.9 keV X-rays (at -30°C) [13, 14]. The minimum detectable energy is 1 keV.

4. Laser system

The laser system [15, 16] is schematically given in Fig. 3 and fulfills following requirements: stochastically triggerable (μ^- enter the gas target at random times) with dead-time smaller than 2 ms, delay between trigger and emission of the light of less than $1 \mu\text{s}$ (given by the 2S lifetime), tunable around $\lambda = 6 \mu\text{m}$ with 0.25 mJ pulse energy and less than 2 GHz bandwidth.

A thin-disk laser pumps a titanium sapphire (TiSa) oscillator-amplifier laser system. Frequency seeding of the TiSa oscillator cavity from a continuous wave (cw) TiSa guarantees frequency control. The 5 ns (FWHM) long pulse emitted from the TiSa laser at 708 nm is then frequency shifted to $6 \mu\text{m}$ with a Raman cell filled with 15 bar of H_2 gas by means of three Stokes processes. The frequency of the pulse exiting the Raman cell is [15]

$$\nu^{\text{output}} = \nu^{\text{TiSa}} - 3 \times \Delta^{\text{Stokes}} \quad (4)$$

where $\Delta^{\text{Stokes}} = 4155.22(2) \text{ cm}^{-1}$ is the vibrational ($0 \rightarrow 1$) transition energy in H_2 [17]. The $6 \mu\text{m}$ pulse is then coupled into a multi-pass cavity surrounding the μ^- stop volume. The light lifetime in this cavity is 50 ns. Laser induced 2 keV X-ray have to be searched in this time window.

Tuning the wavelength of the cw TiSa laser results in a tuning of the frequency of the pulsed TiSa laser by the same amount (due to injection seeding) and a tuning by the same amount at $6 \mu\text{m}$ (see Eq. (4)). The frequency of the cw TiSa laser is known with a precision of 30 MHz. Frequency chirping arising during the pulse formation in the TiSa are $-100(30)$ MHz.

The absolute frequency of the spectroscopy pulse at $6 \mu\text{m}$ has been determined with two different methods. One was performed directly at $\lambda = 6 \mu\text{m}$ by means of water vapor absorption in air and in a cell. This avoids any uncertainties related to chirping effects in the TiSa laser, and to the value of Δ^{Stokes} which is pressure and temperature dependent. The absolute position of the water absorption lines are known to an absolute precision of ~ 1 MHz [18, 19]. The scatter of ~ 30 H₂O absorption line measurements (for 5 different water lines) recorded at various times during the data taking determines the 300 MHz uncertainty of the frequency calibration. This spread arises from pulse-to-pulse instabilities of the Raman process. From this measurement also the spectral width of the pulse has been inferred to be 1.7 GHz.

The second frequency calibration method exploits Eq. (4). Since the frequency of the cw TiSa laser, the chirping effects and Δ^{Stokes} are known it is possible to “indirectly” determine the frequency of the $6 \mu\text{m}$ pulse. The result is in agreement with the direct measurement via water line absorption but less precise due to the uncertainty in the Stoke shift.

5. Measurements

A resonance curve as shown in Fig. 4 is obtained by measuring the number of 1.9 keV X-rays at different laser wavelengths that occur in time-coincidence with the laser pulse. The center of the $2S_{1/2}^{F=1} - 2P_{3/2}^{F=2}$ transition in μp is at 49881.88(76) GHz which corresponds to an energy of $\Delta E_{2S-2P}^{\text{exp}} = 206.2949(32)$ meV [1]. The uncertainty of 15 ppm consists of 700 MHz statistical uncertainty from the free fit of a Lorentzian resonance line on top of a flat background, and the 300 MHz total systematic uncertainty which is exclusively due to the laser wavelength uncertainty. Other systematic effects we have considered are Zeeman shift in the 5 T field

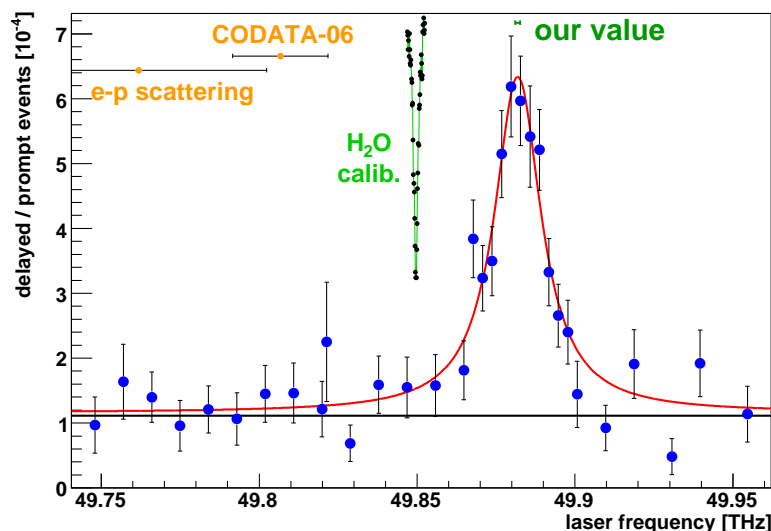


Figure 4. 2S-2P resonance in muonic hydrogen. The number of 2 keV X-rays in coincidence with the laser pulse is plotted as a function of the laser frequency. On resonance we have six events per hour. The predictions (orange points) for the line position assume the proton radius from the CODATA group [8] and from world average electron scattering data [9]. The frequency of the laser is calibrated by means of water line absorption measurements (shown in green).

(< 30 MHz), AC and DC Stark shifts (< 1 MHz), Doppler shift (< 1 MHz) and pressure shift (< 2 MHz). Molecular effects do not influence our resonance position because the formed muonic molecules $pp\mu^+$ are known to deexcite quickly [20] and do not contribute (no 2S population in the molecular state) to our observed signal. Also, the width of our resonance line of 18.0(2.2) GHz agrees with the expected width of 20(1) GHz, whereas molecular lines would be wider.

Concluding, it is important to note that the position of this line strongly disagrees (about four times the linewidth) with theory predictions shown by the orange points in the Fig. 4 (see below).

6. Proton radius from muonic hydrogen Lamb shift

Comparison of the measured transition energy $\Delta E_{2S-2P}^{\text{exp}} = 206.2949(32)$ meV, with the corresponding theoretical prediction based on bound-state QED which account for radiative, recoil, proton structure, fine and hyperfine contributions [2, 3, 4, 5, 6, 7],

$$\Delta E_{2S-2P}^{\text{theo}} = 209.9779(49) - 5.2262 r_p^2 + 0.0347 r_p^3 \quad \text{meV} \quad (5)$$

results in a determination of $r_p = 0.84184(36)^{\text{exp}}(56)^{\text{theo}}$ fm = 0.84184(67) fm. The uncertainty of 0.0049 meV in $\Delta E_{2S-2P}^{\text{theo}}$ is dominated by the proton polarizability term [5] of 0.015(4) meV. A detailed discussion of Eq. (5) is given in the Supplementary Information of Ref [1].

7. Proton radius from H spectroscopy

In a simplified picture, the r_p from H spectroscopy is deduced by comparing the experimentally determined 1S Lamb shift (L_{1S}) with its theoretical prediction. To experimentally determine the 1S Lamb shift at least two transition frequencies need to be measured in H. The transition frequencies are approximately given by the Bohr structure and the Lamb shifts ¹:

$$\left. \begin{array}{l} \nu(1S - 2S) \simeq (1 - \frac{1}{4})R_\infty \frac{m}{m_r} + L_{1S} - L_{2S} \\ \nu(2S - 8S) \simeq (\frac{1}{4} - \frac{1}{64})R_\infty \frac{m}{m_r} + L_{2S} - L_{8S} \\ \vdots \\ L_{nS} = \frac{1}{n^3}L_{1S} + \varepsilon \end{array} \right\} \Rightarrow \begin{array}{l} L_{1S}^{\text{exp}} = 8172.829(19) \text{ MHz} \\ cR_\infty = 3\,289\,841\,960.361(22) \text{ MHz} \end{array} \quad (6)$$

where m is the electron mass, ν 's the transition frequencies and ε a small QED corrections which can be precisely computed. From transition frequency measurements in H both the L_{1S}^{exp} and the R_∞ are determined. From Eq. (6) we see that

$$L_{1S}^{\text{exp}} \approx \frac{8}{7} \left(\nu(1S - 2S) - \frac{3}{4} R_\infty \frac{m}{m_r} \right). \quad (7)$$

$\nu(1S - 2S)$ is measured to a relative accuracy of $u_r = 1.4 \times 10^{-14}$ corresponding to 46 Hz [23], much better than R_∞ whose relative uncertainty is $u_r = 6.6 \times 10^{-12}$ corresponding to 22 kHz [8]. As a consequence, the uncertainty of the experimentally determined Lamb shift $\delta L_{1S}^{\text{exp}}$ originates basically only from the uncertainty of R_∞ which results mainly from the 2S-8S/D and 2S-12S/D transition frequency measurements [29].

The theoretical prediction of the Lamb shift [24, 25, 26, 27, 28, 8] (using $\alpha^{-1} = 137,035999084$ and $B_{60} = -95.3$ [8]) may be expressed as

$$L_{1S}^{\text{theo}} = 8171.636(4) + 1.5645 r_p^2 \quad \text{MHz} \quad (8)$$

¹ The Lamb shift is defined as any deviation from the prediction of the Dirac equation which arises from radiative, recoil, nuclear structure, relativistic and binding effects but excludes leading order recoil and hyperfine contributions [4]. However for simplicity in the following equations we consider it as the deviation from the prediction of the Schrödinger equation. In spite of this, note that the given numerical results refer to the standard definition of the Lamb shift.

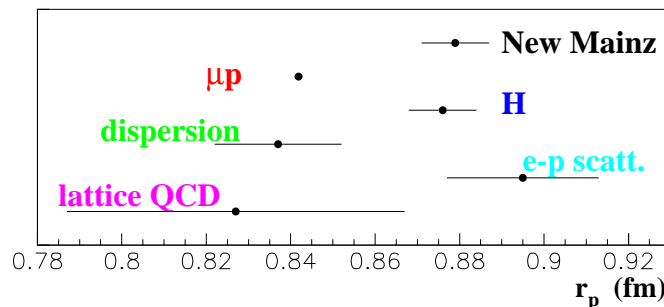


Figure 5. The r_p value from μp spectroscopy is in strong disagreement with the values extracted from H spectroscopy, with the value from the world average electron scattering (e-p scatt.) data [9], and with the new electron scattering value from Mainz [31]. Values from “Lattice QCD” calculations [32], and “dispersion” fit [33] are strongly model dependent.

where the 4 kHz uncertainty arises mainly from the B_{60} term (difference between the perturbative and the all-order approach). Comparing this expression with L_{1S}^{exp} results in $r_p=0.873(8)$ fm, limited by the uncertainty of the latter *i.e.* by δR_∞ .

8. The proton radius puzzle

The proton radii from the various experiments are summarized in Fig. 5. The r_p value from μp is 10 times more precise, but 5.0σ smaller, than the previous best (CODATA) value $r_p = 0.8768(69)$ fm [8], which is mainly obtained from H spectroscopy. It is 26 times more accurate, but 3.1σ smaller, than the previously accepted hydrogen-independent value extracted from electron proton scattering [9, 30] of $r_p = 0.895(18)$ fm. Furthermore it is 4.5σ smaller than the recent results of the MAMI A1 collaboration $r_p = 0.879(8)$ fm [31].

Obviously, the r_p values determined from the various experiments have to be consistent within their accuracies. The observed discrepancy therefore indicates that a problem exists in at least one of the experiments or theory used to extract the radii.

8.1. Is muonic hydrogen experiment wrong?

One way to bring in agreement the r_p value extracted from μp with the one extracted from H and scattering experiment is to shift the frequency of our measurements by 0.3 meV (equivalent to 75 GHz, a relative frequency shift of 0.15%). However, from the experimental point of view a mistake in the frequency calibration or a systematical line shift of 75 GHz has to be excluded. Note that the laser frequency was calibrated with two different methods.

The systematical effects in μp are negligible since generally speaking they scale as $1/m$. For example the Zeeman effect in μp is proportional to the muonic Bohr’s magneton which is 200 times smaller than the standard Bohr’s magneton. Similarly for the pressure shift. The $\mu p(2S - 2P)$ pressure shift in H_2 gas is ~ 1 MHz/hPa [17] whereas it is ~ 100 MHz/hPa for the $H(1S-2S)$. This reduction arises from the smallness of the μp atom (stronger average internal E-field) and larger level splitting. It is also reasonable to question if instead of performing the spectroscopy on a μp atom we have performed spectroscopy on a molecular state. These molecules have been demonstrated to exist [10] but it was demonstrated as well that they have a very short lifetime [20]. Therefore they can not give rise to the measured signal. Furthermore the measured μp linewidth agrees with predictions. The absence of unpredicted broadening is thus an indication of the absence of unknown large systematical shift.

8.2. Is muonic hydrogen theory wrong?

Another possibility to bring in accordance the r_p value extracted from μp with the one extracted from H and scattering experiments would be to correct the $\mu p(2S - 2P)$ theory by 0.3 meV. Such a shift would be equivalent to 60 times the present theory uncertainty of 0.0049 meV.

Many contributions to the $\mu p(2S - 2P)$ splitting have been computed (cf. Supplementary Information of Ref [1]). However the size of the observed discrepancy is larger than all contributions beside the one-loop vacuum polarization (VP), the Källén-Sabry, the leading order HFS, the one-loop muon self-energy and the finite size contribution itself. All other more sophisticated effects as light-by-light, hadronic VP, recoils and proton polarizability contributions are much smaller than the discrepancy. Hence, if the observed discrepancy would originate from the $\mu p(2S - 2P)$ prediction, it would not be caused by a problem of the higher-order contributions but it would be a fundamental problem or it would be related with the one-loop VP or the proton finite size.

It is important to note that the dependence of $\Delta E_{2S-2P}^{\text{theo}}$ on the charge distribution of the proton is small. The finite size contribution given by the term $\sim r_p^2$ in Eq. (5) has been computed assuming a dipole distribution (which fits well the scattering data). If instead a Gaussian shape is assumed, then the finite size effects differ by ~ 500 MHz [5]. The term $\sim r_p^3$ in Eq. (5) is related with the third Zemach moment [21]. Its model dependence is about 500 MHz [5]. Preliminary analysis of new scattering data indicates that the previous value of this contribution has been underestimated [22], but this difference will not resolve the measured discrepancy.

8.3. Are hydrogen theory or experiments wrong?

To conform the r_p from H with our value, the L_{1S}^{theo} or the L_{1S}^{exp} have to be adjusted by about 100 kHz. In fact, inserting our r_p value in the theoretical prediction of Eq. (8) leads to $L_{1S}^{\text{theo}}(r_p^{\mu p}) - L_{1S}^{\text{exp}} \approx 100 (19)^{\text{exp}} (4)^{\text{theo}} (2)^{r_p}$ kHz. Agreement can be thus reestablished if L_{1S}^{exp} (or R_∞) would be shifted by 5 sigma, or if L_{1S}^{theo} would be corrected by more than 15 times the two-loop remainder [28] (equivalent to more than 25 times the uncertainty related with the B_{60} term). Such an energy shift could thus arise only if there is an unexpectedly large three-loop contributions, or a fundamental problem with bound-state QED, or some kind of effects related with the proton which have been neglected.

9. Conclusion and outlook

The observed discrepancy may arise from a computational mistake of the energy levels in μp or H, or a fundamental problem in bound-state QED, an unknown effect related to the proton or the muon, an inconsistent definition of r_p or an experimental error. Speculations related with new particles from keV/c² to few MeV/c² masses with small coupling constants are strongly constrained by spectroscopy of simple atoms [34]. The effect of the weak interaction is negligibly small, and a muon edm (electric dipole moment) of 10^{-18} e-cm (limit from muon $g-2$) would shift the line by 100 MHz. Maybe the discrepancy has unveiled a fundamental problem in bound-state QED which may be significant especially for strong bound-system as μp . For example there is an effort to apply the formalism of [35, 36] to μp and H whose account for “non-local in time” interactions is leading to a new equation of motion and new insight into UV divergences for bound states.

When the observed discrepancy will be solved and if its origin would come from a “simple” computational mistakes or a forgotten effect of “standard” bound-state QED, then the new precise r_p value from μp will pave the way to check H energy level theory to an unprecedented level of accuracy and the radius itself is a interesting benchmark for lattice QCD calculations. In addition our measurement will improve on the determination of the Rydberg constant by a factor of 5 to a level of 1×10^{-12} and on the determination of the deuteron radius via the newly measured isotope shift in H [37] to a level of $u_r = 1 \times 10^{-4}$.

We have presented here only a transition frequency in μp but we have measured a second 2S-2P transition in μp and also 3 transitions in muonic deuterium. The second transition will provide a determination of the Zemach radius with an accuracy of about 3%, whereas the measurement in μd will lead to new determinations of the deuteron radius and the deuteron polarizability and will help to understand the observed proton radius puzzle. A similar measurement of the Lamb shift in muonic helium ions is being prepared at PSI [38]. From this experiment the alpha-particle and the triton radius will be determined with relative accuracies of 10^{-4} . Combined with electron scattering results and an ongoing experiment at MPQ aiming to measure the 1S-2S transition in He^+ it will help to solve the discrepancy and will lead to an enhanced test of the higher-order bound-state QED contributions to He^+ [38]. And clearly all these radii represent benchmarks for lattice QCD and ab-initio few-nucleon theories [39, 40].

Spectroscopy in hydrogen-like atoms continues to challenge our understanding of physics. Muonic hydrogen, deuterium and helium ion in particular, represent interesting platforms to test bound-state theories and to extract nuclear properties.

References

- [1] R Pohl et al., *Nature* **466**, 213 (2010).
- [2] K Pachucki, *Phys. Rev. A* **53**, 2092 (1996).
- [3] K Pachucki, *Phys. Rev. A* **60**, 3593 (1999).
- [4] M I Eides, H Grotch, V A Shelyuto, *Phys. Rep.* **342**, 63 (2001).
- [5] E Borie, *Phys. Rev. A* **71**, 032508 (2005).
- [6] A P Martynenko, *Phys. Rev. A* **71**, 022506 (2005).
- [7] A P Martynenko, *Physics of Atomic Nuclei* **71**(1), 125 (2008).
- [8] P J Mohr, B N Taylor, D B Newell, *Rev. Mod. Phys.* **80**(2), 633 (2008).
- [9] I Sick, *Phys. Lett. B* **576**(1–2), 62 (2003).
- [10] R Pohl et al., *Phys. Rev. Lett.* **97**, 193402 (2006).
- [11] L Ludhova et al., *Phys. Rev. A* **75**, 040501 (2007).
- [12] L M Simons, *Phys. Bl.* **48**, 261 (1992).
- [13] L M P Fernandes et al., *Journal of Instrumentation* **2**, 08005 (2007).
- [14] L Ludhova et al., *Nucl. Instrum. and Meth. A* **540**, 169 (2005).
- [15] A Antognini et al., *Optics Communications* **253**(4-6), 362 (2005).
- [16] A Antognini et al., *IEEE J. Quant. Electr.* **45**(8), 993 (2009).
- [17] A Antognini, Ph.D. Thesis, LMU Munich, Germany (2005), <http://edoc.ub.uni-muenchen.de/5044/>
- [18] R A Toth, *J. Molec. Spectr.* **190**(2), 379 (1998).
- [19] L S Rothman et al., *Journal of Quantitative Spectroscopy and Radiative Transfer* **110**(9–10), 533 (2009).
- [20] S Kilic et al., *Phys. Rev. A* **70**, 042506 (2004).
- [21] J L Friar and I Sick, *Phys. Lett. B* **579** 285-289 (2004).
- [22] M Distler of the MAMI A1 collaboration, Private Communication
- [23] M Niering et al., *Phys. Rev. Lett.* **84**, 5496 (2000).
- [24] K Pachucki and U. D. Jentschura, *Phys. Rev. Lett.* **91**, 113005 (2003).
- [25] U D Jentschura, A. Czarnecki, and K. Pachucki, *Phys. Rev. A* **72**, 062102 (2005).
- [26] U D Jentschura and M Haas, *Can. J. Phys.* **85**, 531 (2007).
- [27] V A Yerokhin, P Indelicato, and V M Shabaev, *Phys. Rev. A* **71**, 040101(R) (2005).
- [28] V A Yerokhin, *Phys. Rev. Lett.* **80**, 040501(R) (2009).
- [29] B de Beauvoir et al., *Eur. Phys. J. D* **12**, 61 (2000).
- [30] P G Blunden, I Sick, *Phys. Rev. C* **72**(5), 057601 (2005).
- [31] J C Bernauer et al., ArXiv nucl-ex (2010), 1007.5076
- [32] P Wang, D B Leineweber, A W Thomas, R D Young, *Phys. Rev. D* 094001 (2009).
- [33] M A Belushkin, H W Hammer, U G Meissner, *Phys. Rev. C* **75**, 035202 (2007).
- [34] S G Karshenboim, *Phys. Rev. Lett.* **104**, 220406 (2010).
- [35] R K Gainutdinov, *J. Phys. A: Math. Gen* **32** 5657-5677 (1999).
- [36] R K Gainutdinov, *Phys. Rev. C*, **66** 014006 (2002).
- [37] C G Parthey et al., *Phys. Rev. Lett.* **104**, 233001 (2010).
- [38] A Antognini et al., submitted to *Can. J. Phys.* (2010).
- [39] P Navrátil et al., *Phys. Rev. Lett.* **99**, 042501 (2007).
- [40] D Gazit et al., *Phys. Rev. Lett.* **103**, 102502 (2009).